

Computational Study of Location and Role of Fluoride in Zeolite Structures

Angeles Pulido, Avelino Corma, and German Sastre*

Instituto de Tecnología Química, UPV-CSIC, Universidad Politécnica de Valencia, Avenida Los Naranjos s/n, 46022 Valencia, Spain

Received: July 7, 2006; In Final Form: September 8, 2006

The distribution of fluoride ions has been studied in the pure silica IFR, ITH, IWR, STF and STT zeolite structures using computational techniques. The interactions between the F^- and SDA^+ ions (where SDA is the organic structure directing agent) are able to explain the F^- cage occupation found experimentally. While studying the short-range fluoride–framework interactions, a relationship was found between the Si atoms forming the pentacoordinated units and the lowest F^- defect energies, which rationalizes the experimental Si–F bonding in terms of energetic stability. It is proposed that the F^- location is governed by a two step process. In a first stage, the electrostatic long-range forces and, especially, the interactions between the F^- and the SDA^+ ions, decide which cage will be filled with F^- ; in a second stage, once the F^- cage location is decided, the F^- forms a covalent bond with a Si site to form an energetically stable pentacoordinated unit $[SiO_4/2F]^-$.

1. Introduction

Zeolites—microporous crystalline aluminosilicates formed by corner-sharing tetrahedral frameworks—find applications in catalysis and separation industrial processes.¹ Much of the recent research in zeolites is focused on the study of their applications and many efforts have been devoted to improving their performance to obtain new or better materials for specific processes.

Zeolites can be synthesized through two different hydrothermal synthetic routes using a hydroxide² or fluoride³ anion as a mineralizer. The nature and properties of the final microporous material can heavily depend on the choice of the anion used as the mineralizer. Thus, high silica zeolites synthesized using the hydroxide route have a significant concentration of connectivity defects due to the need to counterbalance the positive charge of the organic molecules located within the zeolite voids. However, the fluoride route of synthesis has led to the formation of zeolites of high crystallinity and few framework defects.³ The lack of defects in a pure silica zeolite increases the hydrophobicity of the material, which can be important in catalytic applications if elements such as Ti, Fe, Al, or B are used as dopant agents.⁴ Additionally, fluoride ions can determine the phase selectivity during the crystallization.⁵

The introduction of the fluoride anion in the synthesis of zeolites by Flanigen and Patton³ has allowed new structures to be obtained due to the special role played by this anion during synthesis.^{5–10} The fluoride influences the synthesis process in at least two ways. First, it increases the solubility of silica species at neutral pH. Second, it works as a catalyst in the condensation reactions that lead to the formation of Si–O–Si bonds.^{5,11}

Computational techniques,^{12–14} NMR spectroscopy,^{15–19} and X-ray diffraction^{11,20–22} have been used to find the location of fluorine in zeolites. Three general fluoride environments have been reported in pure silica zeolites: (i) Price et al.²³ localized F^- ions in the close proximity to the charged SDA (structure

directing agent) as an ion pair in the main void volume of the zeolite, although this result is subject to some controversy;²⁴ (ii) the F^- ions are separated from the SDA and are located inside small cages in the zeolite framework but not coordinated to any framework atom;²⁵ and (iii) the F^- ions are inside small cages but coordinated to a Si atom, forming a pentacoordinated $[SiO_4/2F]^-$ unit.²¹

Several Si-zeolites such as octadecasil,²⁵ ITQ-7,²⁶ ITQ-13,²⁷ and ITQ-24²⁸ synthesized through the F^- route contain the F^- ion inside a small cage formed by eight tetrahedral atoms named $[4^6]^{29}$ or a double four ring (D4R) unit, where no pentacoordinated silicon exists and the anion is reported to be in the cavity center. Pentacoordinated silicon ($[SiO_4/2F]^-$) units have not been described in D4R units, but they are found in larger cages, like $[4^35^26^1]$, $[4^15^26^2]$, and $[4^35^4]$, present in different pure silica structures such as silicalite (MFI),¹⁷ SSZ-23 (STT),²² ITQ-4 (IFR),³⁰ ferrierite (FER),³¹ ITQ-9 (STF),³² ITQ-13 (ITH),²⁷ SSZ-44 (SFF),³³ and ITQ-24 (IWR).²⁸

The structure of as-made ITQ-4 (IFR) was obtained and refined from high-resolution powder X-ray diffraction (XRD) data, and the organic and fluoride ions have been located by Barrett et al.³⁴ The sinuosity of the channel was found to coincide with the bent geometry observed for the structure directing agent, while the fluoride ions are reported to reside within the $[4^35^26^1]$ cage 2.2 Å from the Si atoms. Pentacoordinated silicon units, $[SiO_4/2F]^-$, were found by Koller et al.¹⁶ using solid-state NMR techniques in various as-made high-silica zeolites (Beta, SSZ-23, ITQ-3, ITQ-4, ZSM-12, and silicalite) prepared in the presence of fluoride ions as a mineralizing agent. Thus, the SSZ-23 (STT), ITQ-4 (IFR), and silicalite (MFI) showed a dynamic motion of the fluoride ions at room temperature which was frozen out at a temperature of 130–140 K. The structure solution and location of fluoride ions inside as-made pure silica zeolites with the IFR and STF framework structures were carried out by Villaescusa et al.³² The long-range ordering of fluoride ions and the pentacoordinated unit, $[SiO_4/2F]^-$, were identified in both zeolites. The relationship between the location of the organic SDAs and fluoride ions was

* E-mail address: gsastre@itq.upv.es. Phone: +34 963 877 803. Fax: +34 963 877 809.

studied, and it was suggested that the location of the fluoride ions could control the orientation of the guest organic molecules.

The local structure of the $[\text{SiO}_{4/2}\text{F}]^-$ unit in fluoride-containing as-synthesized STF zeolites was experimentally determined by Fyfe et al.³⁵ using a combination of solid-state NMR and microcrystal XRD techniques to be very close to trigonal bipyramidal with a Si–F distance of 1.7 Å. The fluoride ions were reported to be disordered between a tetrahedral and five-coordinated environment, giving an apparent Si–F distance longer than expected.

The fluoride ions were reported by Corma et al.²⁷ in the zeolite ITQ-13 (ITH) in two different crystallographic positions. One set located in the center of the D4R cages (two D4Rs per unit cell). However, since the two occluded hexametonium dications give four positive charges per unit cell, two fluoride ions were located inside the $[4^{15}2^6]$ cages with a Si–F distance 1.8 of Å.

The organic structure directing agent and fluoride location were reported in the SSZ-23 (STT) by Cambor et al.²² using XRD techniques. The fluoride ions were located forming pentacoordinated units inside the $[4^35^4]$ cages bonded to silicon atoms with a Si–F distance of 2.0 Å.

Dibenzyltrimethylammonium cations singly fluorinated were investigated by Arranz et al.³⁶ In their study, computer simulations indicate how the electrostatic interactions between the fluoride anions and the organic SDA molecules play a determining role during the crystallization of the microporous material, controlling the orientation of the organic molecules inside the microporous structure.

In an attempt to better understand the role of the fluoride ions during the synthesis of pure silica zeolites, computational techniques were used to study the long-range F^- –SDA⁺ ordering and the short-range fluoride–framework location in the pure silica structures IFR, ITH, STF, and STT, where the fluoride location has been determined experimentally. Moreover, we study the fluoride distribution in the recently synthesized pure silica IWR structure,²⁸ where the fluoride experimental location is not completely known.

2. Methodology

2.1. Force Field Simulation. The calculations have been performed using lattice energy minimization techniques and the GULP code.³⁷ The interatomic potentials used to model the interactions between the atoms in the framework included the following terms: Coulombic interaction, short-range pair potentials (described by a Buckingham function), and a three body bond bending term for the OSiO angles. The shell model was used to simulate the polarizability of the oxygen and fluoride atoms.

In the present work, the total energy, ϵ_{Total} , and the interaction energy between the organic SDAs and the fluoride ions, $\epsilon(\text{F},\text{SDA})$, were evaluated. The total potential energy function and the respective terms are as follows:

$$\epsilon_{\text{Total}} = \epsilon_{\text{zeo}} + \epsilon_{\text{SDA}} + \epsilon_{\text{SDA-SDA}} + \epsilon_{\text{zeo-SDA}} \quad (1)$$

$$\epsilon_{\text{zeo}} = \epsilon_{\text{Buckingham}} + \epsilon_{\text{Coulombic}} + \epsilon_{\text{three-body}} + \epsilon_{\text{core-shell}} \quad (2)$$

$$\epsilon_{\text{Buckingham}} = A_{ij} \exp\left(\frac{r_{ij}}{\rho}\right) - \frac{C_{ij}}{r_{ij}^6} \quad (3)$$

$$\epsilon_{\text{Coulombic}} = \frac{q_i q_j}{r_{ij}} \quad (4)$$

$$\epsilon_{\text{three-body}} = \frac{1}{2} k_{ijk} (\theta_{ijk} - \theta_{ijk}^0)^2 \quad \text{with } \theta = \text{O-Si-O} \quad (5)$$

$$\epsilon_{\text{core-shell}} = \frac{1}{2} k_{i,cs} (r_{i,cs} - r_{i,cs}^0)^2 \quad (6)$$

$$\epsilon_{\text{SDA}} = \epsilon_{ij} + \epsilon_{\text{three-body}} + \epsilon_{ijkl} + \epsilon_{\text{Coulombic}} \quad (7)$$

$$\epsilon_{ij} = \frac{1}{2} k_{ij} (r_{ij} - r_{ij}^0)^2 \quad (8)$$

$$\epsilon_{ijkl} = A_{ijkl} [1 + \cos(n\phi_{ijkl} - \delta_{ijkl})] \quad (9)$$

$$\epsilon_{\text{SDA-SDA}} = \epsilon_{\text{Lennard-Jones}} + \epsilon_{\text{Coulombic}} \quad (10)$$

$$\epsilon_{\text{Lennard-Jones}} = \frac{B_{ij}}{r_{ij}^{12}} - \frac{C_{ij}}{r_{ij}^6} \quad (11)$$

$$\epsilon_{\text{zeo-SDA}} = \epsilon_{\text{Lennard-Jones}} + \epsilon_{\text{Coulombic}} \quad (12)$$

The interaction energy between the F^- and the organic SDA⁺ ions, $\epsilon(\text{F},\text{SDA})$, and the respective terms are as follows:

$$\epsilon(\text{F},\text{SDA}) = \epsilon_{\text{F}} + \epsilon_{\text{SDA}} + \epsilon_{\text{F-F}} + \epsilon_{\text{SDA-SDA}} + \epsilon_{\text{F-SDA}} \quad (13)$$

$$\epsilon_{\text{F}} = \epsilon_{\text{core-shell}} \quad (14)$$

$$\epsilon_{\text{F-F}} = \epsilon_{\text{Buckingham}} + \epsilon_{\text{Coulombic}} \quad (15)$$

$$\epsilon_{\text{F-SDA}} = \epsilon_{\text{Coulombic}} \quad (16)$$

where ϵ_{SDA} and $\epsilon_{\text{SDA-SDA}}$ are described using eqs 7 and 10.

The Ewald summation technique has been used for the summation of the long-range Coulombic interactions. The potentials used for the Si/Ge/F zeolites¹³ have been demonstrated to successfully model the structure and vibrations associated to F^- of octadecasil²⁵ and the structures of SSZ-35 and SSZ-44.³⁸ Furthermore, this potential is able to give valuable information about the structure of Si/Ge/F zeolites.^{39,40} The force field by Kiselev et al.⁴¹ was selected for the intermolecular SDA–zeolite and SDA–SDA interactions, and the intramolecular SDA interactions were modeled with the force field by Oie et al.⁴² More details on the computational methods can be found elsewhere.^{43–48}

We employed the Mott–Littleton methodology to treat the incorporation of defects within the perfect lattice. This widely used method allows the full relaxation of atomic coordinates of an inner region (100–500 atoms), surrounding the defect, to minimum energy, while more distant regions of the crystal are treated as a dielectric continuum. Thus, with the introduction of only one fluoride ion in the void volume of the framework to get the defect energy, it is possible to analyze the interaction between the F^- ions and the zeolite framework due to the fact that no SDA molecules are hosted in the zeolite.

2.2. Models. **2.2.1. Unit Cells.** The structures IFR, ITH, IWR, STF, and STT were used to study the factors that can be involved in the distribution of fluoride anions in pure silica zeolites. The calculations were performed using as unit cells:

(i) $[\text{BQ},\text{F}]_2\text{-Si}_{32}\text{O}_{64}$ for the IFR structure, where BQ is benzylquinuclidinium, the organic structure directing agent

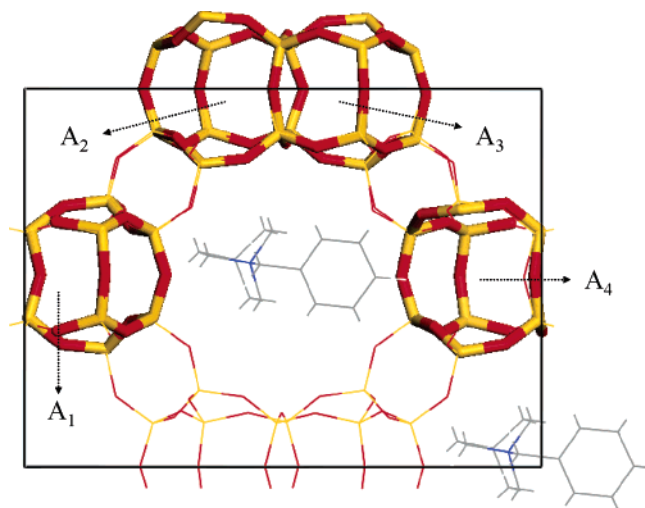


Figure 1. Optimized unit cell of the IFR structure, $[\text{BQ},\text{F}]_2\text{-Si}_{32}\text{O}_{64}$, where the four $[4^35^26^1]$ cages (A_1 , A_2 , A_3 , and A_4) per unit cell are highlighted. The fluoride ions have been omitted for the sake of clarity.

TABLE 1: Number of Cages Per Unit Cell in the Structures IFR, ITH, IWR, STF, and STT^a

structure	$[4^6]^b$	$[4^25^4]$	$[4^26^4]$	$[4^15^26^2]$	$[4^35^26^1]$	$[4^35^4]$	$[4^35^46^1]$
IFR					4		
ITH	2		4	4			
IWR	2	4	4	4			
STF				4			
STT						4	4

^a The number of SiO_2 units per unit cell in each structure is 32, 56, 56, 32, and 64, respectively. ^b The $[m^n\dots]$ cage notation indicates n windows formed by m tetrahedral, T, atoms.

reported by Villaescusa et al.³² in their study of the fluoride location in the pure silica structure IFR (zeolite ITQ-4⁴⁹);

(ii) $[\text{HEX},\text{F}_2]_2\text{-Si}_{56}\text{O}_{112}$ for the ITH structure, where HEX is hexametonium, the organic structure directing agent reported in the synthesis of pure silica ITH structure (zeolite ITQ-13²⁷);

(iii) $[\text{DECA},\text{F}_2]_2\text{-Si}_{56}\text{O}_{112}$ for the IWR structure, where DECA is 4,8-(2-methyl)-ethenobenzo[1,2-c:4,5-c']dipyrrolium-4-methyl-2,2,6,6-tetraethyl-1,2,3,3a,4a,5,6,7,7a,8a-decahydro, the structure directing agent reported in the synthesis of pure silica IWR structure²⁸ (zeolite ITQ-24⁵⁰);

(iv) $[\text{DMABO},\text{F}]_2\text{-Si}_{32}\text{O}_{64}$ for the STF structure, where DMABO is *N,N*-dimethyl-6-azonium-1,3,3-trimethylbicyclo-(3.2.1)-octane, the organic structure directing agent reported by Villaescusa et al.³² in their study of the fluoride location in the pure silica structure STF (zeolite SSZ-35⁵¹);

(v) $[\text{TMAda},\text{F}]_4\text{-Si}_{64}\text{O}_{128}$ for the STT structure, where TMAda is *N,N,N*-trimethyl-1-adamantammonium, the organic structure directing agent reported in the synthesis of the pure silica STT structure (zeolite SSZ-22²²).

2.2.2. Cage Description. The IFR structure is a one-dimensional zeolite characterized by its channel containing pore openings of twelve tetrahedral atoms (12-ring) parallel to the *c* crystallographic direction. Around the perimeter of the channels there are $[4^35^26^1]$ cages, and two cages are fused sharing a common four-member ring (4MR) face (see Figure 1). There are four $[4^35^26^1]$ cages in the unit cell of the IFR structure: A_1 , A_2 , A_3 , and A_4 , where the fusion of the A_1 cage with the A_4 cage and the A_2 cage with the A_3 cage is shown, (see Figure 1 and Table 1).

The ITH structure exhibits intercrossed medium-pore channels; a 9-ring channel runs parallel to the crystallographic *a* axis, another 10-ring set of channels runs parallel to the *b* axis,

and parallel to the *c* axis cavities containing windows of 10 rings are present. There are three cages in the ITH structure where the fluoride ions are located: (i) $[4^6]$ cages (two per unit cell), named double four ring (D4R), (ii) $[4^15^26^2]$ cages (four per unit cell), (iii) $[4^26^4]$ cages (four per unit cell); see Figure 2 and Table 1.

The IWR structure presents a tridirectional pore system of intercrossing 12- and 10-ring channels. The first set of 12-ring straight channels runs perpendicularly to the *ab* plane. A second set of 12-ring sinusoidal channels runs along the *a* axis. Finally, there is a 10-ring channel system that intersects perpendicularly to both 12-ring channels (see Figure 3). There are four different cages where the fluoride ions are placed: (i) $[4^6]$ cages (two cages per unit cell), (ii) $[4^25^4]$ cages (four cages per unit cell), (iii) $[4^15^26^2]$ cages (four per unit cell), and (iv) $[4^26^4]$ cages (four cages per unit cell); see Figure 3 and Table 1.

The STF structure shows an unusual one-dimensional straight channel which contains pore openings that alternate between rings of 10 and 18 tetrahedral atoms (10- and 18-ring) and runs parallel to the *c* axis. Analogously to the IFR structure, $[4^15^26^2]$ cages are around the perimeter of the channel (see Figure 4). Two fluorides neutralize the charged SDAs, and there are four $[4^15^26^2]$ cages per unit cell, named B_1 , B_2 , B_3 , and B_4 , (see Figure 4 and Table 1).

The STT structure presents a channel, which runs parallel to the *c* axis, bounded at the narrowest points by 7-ring windows. Parallel to the $[101]$ direction are the channels bounded by 9-ring windows, slightly offset against each other. There are two types of cages, $[4^35^4]$ (four per unit cell) and $[4^35^46^1]$ (four per unit cell), located at the intersection of the 7- and 9-ring channels (see Figure 5 and Table 1).

2.3. F⁻ Distributions and Energetics. How should $x\text{F}^-$ ions be distributed in y cages ($y \geq x$)? We separate possible configurations into what we call “distribution sets”, which are configurations with F^- restricted into certain cage types (see Table 2). For a given distribution set, a significant number of random configurations is generated and its energy is calculated. The energy of such a distribution set is the Boltzmann weighted summation as follows:

$$E_{\text{Total}} = \sum_i v_i \epsilon_{\text{Total},i} \quad (17)$$

where the probability v_i is

$$v_i = \frac{e^{-\epsilon_{\text{Total},i}/kT}}{\sum_j e^{-\epsilon_{\text{Total},j}/kT}} \quad (18)$$

Analogously, the interaction energy between the F^- and SDA^+ ions (including all the terms show in eq 13) corresponding to each distribution, $E(\text{F},\text{SDA})$, was calculated as follows:

$$E(\text{F},\text{SDA}) = \sum_i w_i \epsilon_i(\text{F},\text{SDA}) \quad (19)$$

where the probability w_i is

$$w_i = \frac{e^{-\epsilon_i(\text{F},\text{SDA})/kT}}{\sum_j e^{-\epsilon_j(\text{F},\text{SDA})/kT}} \quad (20)$$

3. Results and Discussion

3.1. F⁻ Distributions in IFR, ITH, STF, and STT Structures. The organic SDAs were located within the main void

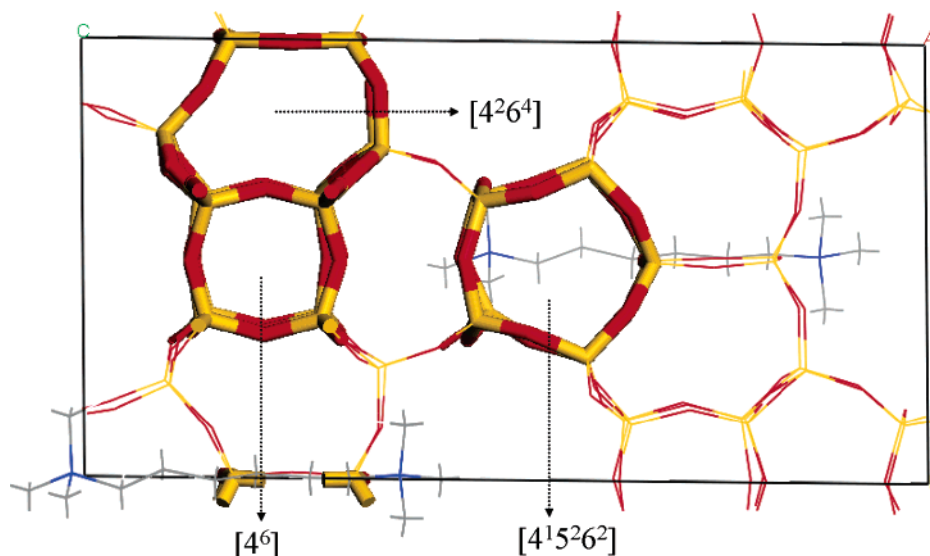


Figure 2. Optimized unit cell of the ITH structure, $[\text{HEX},\text{F}_2]_2\text{-Si}_{56}\text{O}_{112}$, where the $[4^6]$, $[4^{15}5^62]$, and $[4^26^4]$ cages are highlighted. The fluoride ions have been omitted for the sake of clarity.

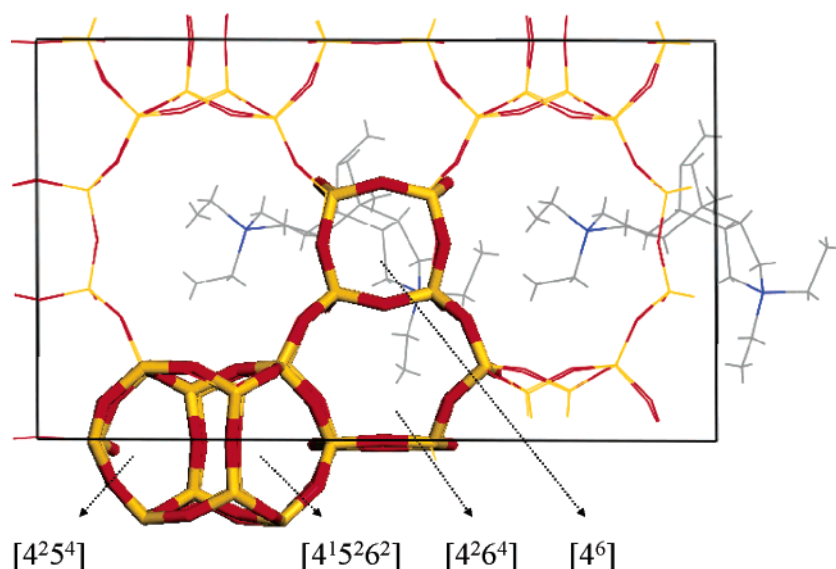


Figure 3. Optimized unit cell of the IWR structure, $[\text{DECA},\text{F}_2]_2\text{-Si}_{56}\text{O}_{112}$, where the $[4^6]$, $[4^25^4]$, $[4^{15}5^62]$, and $[4^26^4]$ cages are highlighted. The fluoride ions have been omitted for the sake of clarity.

volume of the zeolite frameworks; see Figures 1–5. The fluoride ions were placed within the different cages of the zeolite frameworks, and different sets of random fluoride distributions were generated (see Table 2). First, a full geometry optimization was performed to obtain the total energy of the unit cells, ϵ_{Total} (from eq 1). A Boltzmann weighting of all these energies gives us the E_{Total} (from eq 17). Afterwards, with the aim to investigate the role of the long-range interactions between the F^- and the SDA^+ ions (including all the terms shown in eq 13) in the fluoride distribution, in pure silica zeolites, we obtained the interaction energy between the fluoride and the organic SDAs ions, $E(\text{F},\text{SDA})$ (from eqs 13 and 19), using the optimized geometries. Then, we would like to see whether the experimental F^- distributions in IFR, ITH, STF, and STT can be explained by either or both of the energies calculated, E_{Total} and $E(\text{F},\text{SDA})$.

3.1.1. ITH Structure. The four fluoride ions present in the unit cell, $[\text{HEX},\text{F}_2]_2\text{-Si}_{56}\text{O}_{112}$, were distributed randomly in three different sets, as follows: (i) fluoride ions inside any of the three types of cages (D4R, $[4^{15}5^62]$, and $[4^26^4]$), distributions named ITH-cage, (ii) two of the fluoride ions located in the two D4R cages and the other two anions inside the $[4^26^4]$ cage,

distributions named ITH-D4R-cage, and (iii) two of the fluoride ions locate inside the two D4R and the other two fluoride ions distributed between the four cages $[4^{15}5^62]$, distributions named ITH-D4R- $[4^{15}5^62]$. A schematic description of the distribution sets generated is indicated in Table 2.

A total number of 900 configurations (300 per distribution set) were optimized and subsequently the $E(\text{F},\text{SDA})$ energy was calculated using eqs 13 and 19. The results are displayed in Table 3 where the different distribution sets are indicated. From Table 3, it is seen that the lowest energy values arise from distributions where two out of the four fluoride ions in the unit cell are located in the D4R units, ITH-D4R-cages, and ITH-D4R- $[4^{15}5^62]$ distributions. A more careful inspection of Table 3 shows that the lowest energy values arise from the ITH-D4R- $[4^{15}5^62]$ distribution set, -6.8 eV, whereas the ITH-D4R-cage distribution shows an intermediate value, -6.3 eV, and the highest value is observed for the ITH-cage, -6.0 eV. It is worth noting that the location of fluoride ions found experimentally in the ITQ-13 zeolite²⁷ corresponds to the ITH-D4R- $[4^{15}5^62]$ distribution set (see Table 4 for details) as predicted from our lowest energy configuration. This means that, per unit cell, two

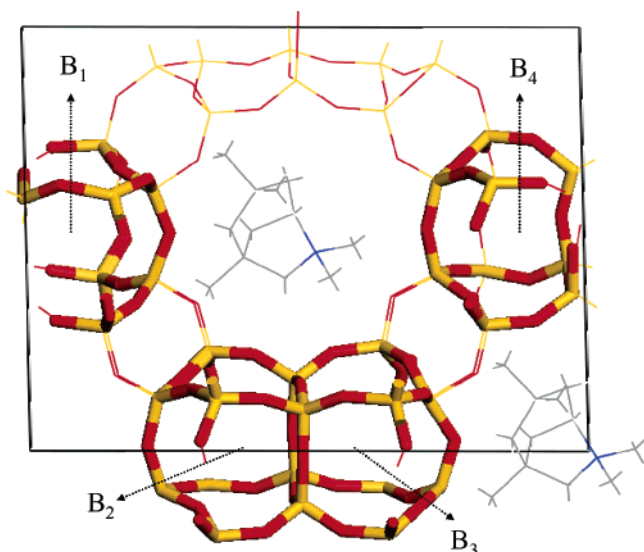


Figure 4. Optimized unit cell of the STF structure, [DMABO,F]₂–Si₃₂O₆₄, where the four [4¹⁵26²] cages (B₁, B₂, B₃, and B₄) per unit cell are highlighted. The fluoride ions have been omitted for the sake of clarity.

F[−] ions are located in D4R and two F[−] ions are in [4¹⁵26²] cages. From the results, this would indicate that the energy $E(\text{F},\text{SDA})$ is a good criteria to predict the experimental F[−] location.

We have rationalized the fluoride experimental distribution in the pure silica ITH structure using the $E(\text{F},\text{SDA})$ energy, regardless the total energy, E_{Total} , and this indicates the importance of the electrostatic contribution to the F[−] cage location. Thus, to confirm if the electrostatic long range forces and, especially, F–SDA interactions (including all the terms show in eq 13) are controlling the F[−] cage occupation in pure silica zeolites, we use the same methodology to study the role of the $E(\text{F},\text{SDA})$ energy, in the fluoride distribution of the other pure silica structures.

3.1.2. STT Structure. Two different sets were generated distributing the four fluoride ions present in the unit cell, [TMAda,F]₄–Si₆₄O₁₂₈, as follows: (i) fluoride ions located inside the [4³⁵4] cages, named the STT-[4³⁵4] set and (ii) fluoride anions sited inside the [4³⁵46¹] cages, named the STT-[4³⁵46¹] set (see Table 2). Here, 600 configurations (300 per distribution set) were generated, and the full geometry optimization was performed for each one. The $E(\text{F},\text{SDA})$ energy was calculated (from eqs 13 and 19) using the optimized geometry and the results are displayed in Table 3. Among the two fluoride ion distributions studied, STT-[4³⁵4] and STT-[4³⁵46¹], the lowest $E(\text{F},\text{SDA})$ energies corresponded to the STT-[4³⁵4] distribution set, −11.1 eV, while the value observed for the STT-[4³⁵46¹] distribution is −10.3 eV; see Table 3. Experimentally, the fluoride anion in the zeolite SSZ-23 has been found inside the [4³⁵4] cages;^{22,52} see Table 4. As in the previous case studied, i.e., the ITH structure, the experimental fluoride distribution is predicted from the lowest $E(\text{F},\text{SDA})$ configuration. Thus, it is possible to rationalize the fluoride location in pure silica ITH and STT structures by analyzing the interaction energy between the fluoride and the organic SDA ions (including all the terms show in eq 13) regardless the framework stability and the total energy, E_{Total} .

We now study the fluoride location in ITQ-4 (IFR) and SSZ-35 (STF) zeolites to test our model and to locate and rationalize fluoride positions in pure silica zeolites. These zeolites have similar structural features, as they both contain fused small cages

arranged into columns generating one-dimensional channels (see Figures 1 and 4). In the case of the ITQ-4 zeolite, the structure determination revealed that the material is noncentrosymmetric and polar despite the centrosymmetric nature of the framework (IFR structure). Moreover, the hypothesis that similar structural features of SSZ-35 (STF) would lead to a similar noncentrosymmetric ordering as seen in IFR was proven to be incorrect.³² In both cases, the symmetry nature of the material and the F[−] location are influenced by the SDA ordering; therefore, it is interesting to study the fluoride distribution in the IFR and STF structures.

3.1.3. IFR Structure. The two fluoride ions present in the unit cell were distributed between the four [4³⁵26¹] cages (A₁, A₂, A₃, and A₄ in Figure 1) in six different distribution sets: (i) if the fluoride ions are located inside the A₁ and the A₂ cages, the distributions are named IFR-A₁-A₂; (ii) when the fluoride ions are place inside the A₁ and A₃ cages, the distributions are referred to as IFR-A₁-A₃; (iii) if the occupied cages are A₁ and A₄, then we get the IFR-A₁-A₄ distributions; (iv) when the cages A₂ and A₃ host the fluoride ions, then the IFR-A₂-A₃ set is generated; (v) if the fluoride anions sited in the A₂ and A₄ cages, then IFR-A₂-A₄ distributions are obtained; and (vi) the distribution IFR-A₃-A₄ is where the cages A₃ and A₄ are occupied (see Table 2). We generate randomly a total of 600 configurations, 100 configurations for each distribution set. The calculated $E(\text{F},\text{SDA})$ values for the IFR structure, [BQ,F]₂–Si₃₂O₆₄, are displayed in Table 3. The $E(\text{F},\text{SDA})$ values show an interesting ordering which was not observed in the previous cases studied (ITH and STT structures). The lowest $E(\text{F},\text{SDA})$ energies are observed for the IFR-A₁-A₃ and IFR-A₂-A₄ distribution sets, −2.6 and −2.3 eV, respectively. These distributions represent the fluoride location where the fluoride–fluoride distances are the largest due to F[−] located inside alternate cages, (A₁ alternates with A₃, and A₂ alternates with A₄; see Figure 1). The term *alternate* will be used to denote this spatial distribution. The IFR-A₁-A₂ and the IFR-A₃-A₄ sets form the second energy group (−2.0 and −2.2 eV, respectively) in Table 3, where the fluoride ions are placed inside close cages and this spatial situation is called *close* (see Figure 1). Finally, the highest $E(\text{F},\text{SDA})$ values are displayed for the IFR-A₁-A₄ and IFR-A₂-A₃ distribution sets (−1.7 and −1.5 eV, respectively), which represent the closest fluoride positions, and due to that, in these distributions, the fluoride ions are sited inside *fused* cages (see Figure 1). So, in the IFR structure, apart from the attractive F[−]–SDA⁺ term, the repulsive F[−]–F[−] interactions are also controlling the fluoride distribution through the fluoride–fluoride distance.^{16,32,34} We would like to highlight the fact that the energetic term that we are considering, $E(\text{F},\text{SDA})$, contains the electrostatic contributions not only of the F–SDA, but also F–F (among others), as can be seen from eq 13, and therefore, the role of the F–F interactions is taken into account when evaluating the $E(\text{F},\text{SDA})$ energy. Thus, the experimental F[−] occupation, IFR-A₁-A₃, has been predicted from our lowest energy configuration. Again, a relationship between experimental fluoride distribution and minimum $E(\text{F},\text{SDA})$ energy has been found (see Table 4).

3.1.4. STF Structure. The two fluoride ions present in the unit cell were distributed between the four [4¹⁵26²] cages in six different distributions: (i) when the fluoride ions are located inside the B₁ and the B₂ cages, the set is named STF-B₁-B₂; (ii) if the fluoride ions are place inside the B₁ and B₃ cages, the distribution is referred to as the STF-B₁-B₃ set; (iii) if the occupied cages are B₁ and B₄, then we get the STF-B₁-B₄ distribution set; (iv) when the cages B₂ and B₃ host the fluoride ions, then the STF-B₂-B₃ set is generated; (v) if the fluoride

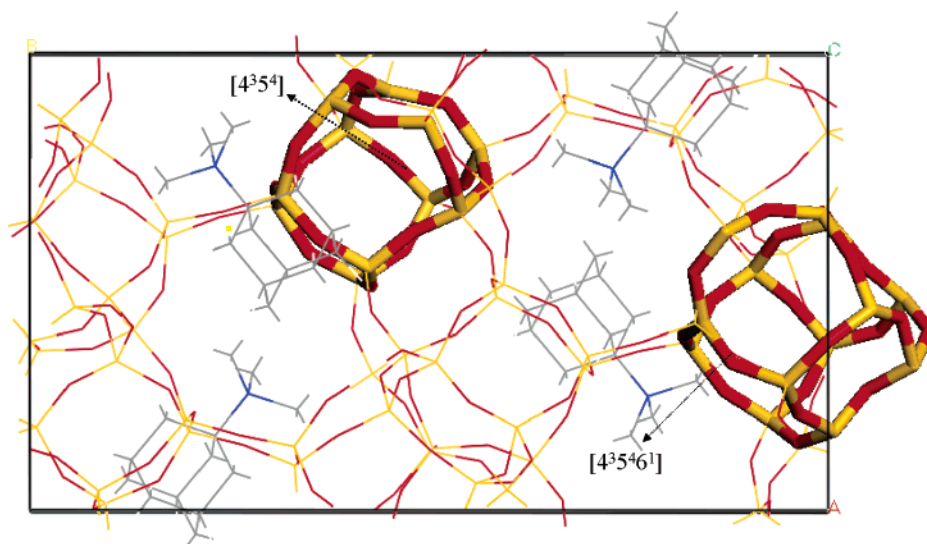


Figure 5. Optimized unit cell of the STT structure, $[\text{TMAda},\text{F}]_4\text{-Si}_{64}\text{O}_{128}$, where the $[4^3 5^4]$ and $[4^3 5^4 6^1]$ cages are highlighted. The fluoride ions have been omitted for the sake of clarity.

TABLE 2: Distribution Sets and Number of Configurations Calculated per Each Set for the Structures IFR, ITH, IWR, STF, and STT^d

structure	distribution set ^a	$[4^6]^b$	$[4^2 5^4]$	$[4^2 6^4]$	$[4^1 5^2 6^2]$	$[4^3 5^2 6^1]$	$[4^3 5^4]$	$[4^3 5^4 6^1]$	N_F	no. of configs
IFR	IFR-A ₁ -A ₂					2		2		100
	IFR-A ₁ -A ₃					2		2		100
	IFR-A ₁ -A ₄					2		2		100
	IFR-A ₂ -A ₃					2		2		100
	IFR-A ₂ -A ₄					2		2		100
	IFR-A ₃ -A ₄					2		2		100
ITH	ITH-cage	N_1		N_2	N_3			$N_1 + N_2 + N_3 = 4^c$		300
	ITH-D4R-cage	2		2	0			4		300
	ITH-D4R- $[4^1 5^2 6^2]$	2		0	2			4		300
IWR	IWR- $[4^2 5^4]$		4					4		100
	IWR- $[4^2 6^4]$			4				4		100
	IWR- $[4^1 5^2 6^2]$				4			4		100
	IWR-D4R- $[4^2 5^4]$	2	2					4		100
	IWR-D4R- $[4^2 6^4]$	2		2				4		100
	IWR-D4R- $[4^1 5^2 6^2]$	2			2			4		100
STF	STF-B ₁ -B ₂				2			2		100
	STF-B ₁ -B ₃				2			2		100
	STF-B ₁ -B ₄				2			2		100
	STF-B ₂ -B ₃				2			2		100
	STF-B ₂ -B ₄				2			2		100
	STF-B ₃ -B ₄				2			2		100
STT	STT- $[4^3 5^4]$						4	4		300
	STT- $[4^3 5^4 6^1]$							4	4	300

^a The distribution set indicates the cages where F^- locates. For example, IFR-A₁-A₂ means that the F ions are located exclusively in cavities A₁ and A₂ (see Figure 1). ^b The $[m^n \dots]$ cage notation indicates n windows formed by m tetrahedral, T, atoms. ^c The N_1, N_2, \dots notation was used to indicate the total number of fluoride ions distributed in the cages. ^d The total number of F^- per unit cell, N_F , and the number of F^- distributed inside each cage are indicated below the corresponding cage label.

anions are sited in the B₂ and B₄ cages, then the STF-B₂-B₄ distribution set is obtained; and (vi) the last distribution set is the STF-B₃-B₄ where the cages B₃ and B₄ are occupied (see Table 2). We generate randomly a total number of 600 configurations, 100 configurations for each distribution set.

The calculated $E(\text{F},\text{SDA})$ values, using the optimized geometries, for the STF structure, $[\text{DMABO},\text{F}]_2\text{-Si}_{32}\text{O}_{64}$, are displayed in Table 3. As the IFR structure, it is possible to order the $E(\text{F},\text{SDA})$ values according to the alternate, close, and fused cage distributions (see Table 3). The highest energies are observed for the fluoride distribution inside fused cages, STF-B₁-B₄ and STF-B₂-B₃ sets, -8.9 and -8.9 eV, respectively. The distribution sets where the fluoride ions are located inside close cages, STF-B₁-B₂ and STF-B₃-B₄, present lower $E(\text{F},\text{SDA})$ energies (-9.6 and -9.8 eV, respectively) than fused cage distributions (-8.9 and -8.9 eV). The lowest $E(\text{F},\text{SDA})$ values

are shown for alternate cage distributions, STF-B₁-B₃ and STF-B₂-B₄ (-9.9 and -10.3 eV). Thus, apart from the F-SDA interactions, the fluoride-fluoride interactions represent an important controlling factor in the location of fluoride ions in the STF structure. The fluoride distribution in the STF structure proposed by Villaescusa et al.³² precludes two fluoride ions from being attached to the same four ring (a special case of a close cage configuration) and also precludes two fluoride ions from being inside fused cages (see Figure 4). Fyfe et al.,³⁵ using NMR techniques, confirm the proposal that the fluoride ions do not occupy both cages of the fused unit due to unfavorable electrostatic repulsions. Thus, it is possible to use the $E(\text{F},\text{SDA})$ energy as a useful tool in the rationalization of the fluoride distribution in pure silica zeolites. The lowest $E(\text{F},\text{SDA})$ energies are shown (Table 3) for distributions which correspond to those

TABLE 3: $E(\text{F},\text{SDA})$ Energies, Using Equations 13 and 19 in the Pure Silica ITH, STT, IFR, STF, and IWR Structures

structure	distribution set ^a	$E(\text{F},\text{SDA})$ (eV)
ITH	ITH-cage	-6.0
	ITH-D4R-cage	-6.3
	ITH-D4R-[4 ¹ 5 ² 6 ²]	-6.8
STT	STT-[4 ³ 5 ⁴]	-11.1
	STT-[4 ³ 5 ⁴ 6 ¹]	-10.3
IFR	IFR-A ₁ -A ₂	-2.0
	IFR-A ₁ -A ₃	-2.6
	IFR-A ₁ -A ₄	-1.7
	IFR-A ₂ -A ₃	-1.5
	IFR-A ₂ -A ₄	-2.3
	IFR-A ₃ -A ₄	-2.2
	IFR-B ₁ -B ₂	-9.6
STF	STF-B ₁ -B ₃	-9.9
	STF-B ₁ -B ₄	-8.9
	STF-B ₂ -B ₃	-8.9
	STF-B ₂ -B ₄	-10.3
	STF-B ₃ -B ₄	-9.8
	STF-B ₄ -B ₃	-9.8
IFR	IFR-CH-A ₁ -A ₂	-2.1
	IFR-CH-A ₁ -A ₃	-2.7
	IFR-CH-A ₁ -A ₄	-1.9
	IFR-CH-A ₂ -A ₃	-1.6
	IFR-CH-A ₂ -A ₄	-2.9
	IFR-CH-A ₃ -A ₄	-2.2
IWR	IWR-[4 ² 5 ⁴]	-0.4
	IWR-[4 ² 6 ⁴]	-0.9
	IWR-[4 ¹ 5 ² 6 ²]	-0.9
	IWR-D4R-[4 ² 5 ⁴]	-2.4
	IWR-D4R-[4 ² 6 ⁴]	-2.2
	IWR-D4R-[4 ¹ 5 ² 6 ²]	-2.4
	IWR-D4R-[4 ¹ 5 ² 6 ²]	-2.4

^a Distribution set labeling from Table 2.

observed experimentally and the highest energies correspond to distributions not observed.

Now, we study the reason fluoride anions have such different distributions in the IFR and STF structure despite their structural similarity. In both cases, the alternate cage distributions show the lowest energy values; however, in the IFR structure, the IFR-A₁-A₃ distribution is the lowest, whereas in the STF structure the IFR-B₂-B₄ set is the lowest. If we accept a similar fluoride-fluoride repulsion between alternate cage distributions arising from the same structure, it is then necessary to study deeply the role of the organic SDAs. From Figure 1, it is possible to see the SDA phenyl group, inside the IFR structure, located closest to the A₄ cage, which would interact repulsively with the fluoride anion sited in this cage, whereas the IFR-A₁-A₃ distribution shows an *alternate* cage distribution and a longer phenyl-fluoride distance. So, we think that the repulsive interaction between the fluoride ions and the aromatic group of the organic SDA will preclude the A₄ cage to be occupied in the IFR structure and only the IFR-A₁-A₃ distribution would be permitted. However, there is no restriction in fluoride distribution in alternate cages in the STF structure, where no aromatic SDA was used in the synthesis, and then, both alternate distributions (STF-B₁-B₃ and STF-B₂-B₄) are present.

To test the role of the aromatic group in the synthesis of the pure silica IFR structure, we study the fluoride distribution in the IFR structure when the CH (where CH is the nonaromatic BQ analogue) is used as a structure directing agent during the simulations. Thus, we repeat the $E(\text{F},\text{SDA})$ calculations in the IFR structure with the unit cell: $[\text{CH},\text{F}]_2\text{-Si}_{32}\text{O}_{64}$. The distributions will be named as in the previous IFR simulations, so the IFR-CH-A_i-A_j distribution set represents the distribution of two fluoride ions in the A_i and A_j cages where CH is used as an SDA instead of the reported BQ. The $E(\text{F},\text{SDA})$ energies were calculated from the optimized geometries and displayed in Table 3. The general trends are kept when using CH as an SDA, and

it is possible to see the same ordering distribution. However, the lowest energy values are shown for the IFR-CH-A₂-A₄ distribution, -2.9 eV, instead of the IFR-CH-A₁-A₃, -2.7 eV, observed when BQ was used as the SDA. Thus, when a nonaromatic SDA is used in the simulation of the IFR structure, the fluoride distribution is closer to that of STF. Therefore, the use of an aromatic SDA in the synthesis of the pure silica STF structure would lead to a similar distribution to that observed in the IFR structure and could be used to constrain the fluoride location.

It is interesting to note that the organic SDAs, HEX and BQ, were located in the main void volume of the ITH and IFR structures, respectively, being ordered as observed in the experiments.^{27,32} Nevertheless, the organic SDA, DMABO, used in the simulation of the STF structure is assumed to be perfectly ordered, from one unit cell to the next one, where the SDA hosted in the STF structure does not experimentally show such ordering.³² However, the F⁻ location seems to be close to the experimental description, and we think that no artificial ordering of the F⁻ anions is being created using such SDA ordering in the simulations.

One of the most intriguing question in the study of the role of the F⁻ anion in the synthesis of zeolite materials is the reason that several cages are present in the structure in which the F⁻ is located preferentially in small cages and especially in the D4R. We think it is interesting to note that it is possible to explain the preferential location of F⁻ anions in the D4R units attending only to the F-SDA interactions using the $E(\text{F},\text{SDA})$ where no structural factors are involved. Attending to this fact, could it be possible to use the F-SDA interactions to prevent the F⁻ location in the D4R units? Could an SDA of similar shape but different charge distribution be used to get the same zeolite structure but with a different F⁻ distribution and no F⁻ located inside the D4R unit? We think that this certainly could stimulate some interesting ideas about template design to test this premise.

3.2. Insights into the F⁻ Distribution in the IWR Structure. Recently, in our group, the pure silica IWR structure (zeolite ITQ-24) has been synthesized using DECA (4,8-(2-methyl)-ethenobenzo[1,2-c:4,5-c']dipyrrolium-4-methyl-2,2,6,6-tetraethyl-1,2,3,3a,4a,5,6,7,7a,8a-decahydro) as an SDA.²⁸ Three ¹⁹F magic-angle spinning (MAS) NMR signals were observed at -38, -59, and -81 ppm, with a relative intensity of 1.00, 0.54, and 0.09, respectively. The signal at -38 ppm was assigned to F⁻ ions located in the D4R units (two atoms per unit cell), and the peaks at -59 and -81 ppm were reported to be arising from 1 F⁻ probably located in the [4²5⁴] cage and 0.18 F⁻ in the [4²6⁴] cages. Now, the previously established correlation between $E(\text{F},\text{SDA})$ and the fluoride distribution in the structures IFR, ITH, STF, and STT was used to try to explain the fluoride distribution in the pure silica IWR structure.

The four fluoride ions present in the IWR unit cell, $[\text{DECA},\text{F}_2]_2\text{-Si}_{56}\text{O}_{112}$, were distributed between the four different types of cages present in the IWR structure. To analyze the location of fluoride ions, six distribution sets were studied: (i) the fluoride ions were placed inside the [4²5⁴] cages, named the IWR-[4²5⁴] distribution; (ii) the fluoride anions located inside the [4¹5²6²] cages, called the IWR-[4¹5²6²] distribution; (iii) the fluoride sited in the [4²6⁴] cages, named the IWR-[4²6⁴] distribution; (iv) two fluoride ions in the two D4R units present in the unit cell and the other two fluoride inside [4²5⁴] cages, named the IWR-D4R-[4²5⁴] distribution; (v) two fluorides located in D4R units and two inside [4¹5²6²] cages, named the IWR-D4R-[4¹5²6²] distribution; (vi) two fluoride inside D4R

TABLE 4: Fluoride Incorporation Energy, E_{def} (eV), in the Pure Silica ITH, STT, IFR, and STF Structures^e

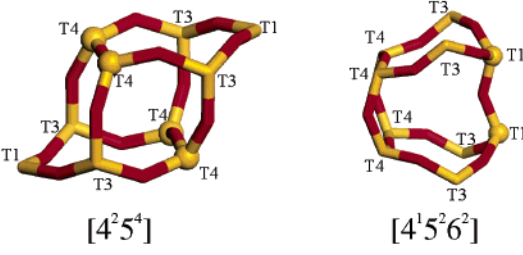
structure	cage ^a	Si ^b	E_{def} (eV) ^c	experimental F ⁻ location and references ^d	
ITH	D4R	Si2	-3.7	 [27]	
		Si5	-3.7		
	[4 ¹ 5 ² 6 ²]	Si6	-3.0		
		Si7	-3.1		
		Si9	-3.0		
STT	[4 ³ 5 ⁴]	Si4	--	 [16], [22], [52]	
		Si5	--		
		Si6	-3.2		
		Si7	-3.2		
		Si9	-3.1		
		Si11	--		
		Si12	-3.1		
		Si13	-3.2		
		Si14	-2.9		
		Si15	-2.6		
IFR	[4 ³ 5 ² 6 ¹]	Si1	-2.8	 [16], [32], [34]	
		Si2	-3.1		
		Si3	-3.2		
		Si4	-3.2		
STF	[4 ¹ 5 ² 6 ²]	Si1	-3.1	 [32], [35]	
		Si2	-3.2		
		Si3	-3.2		
		Si4	-3.1		
		Si5	-3.0		

^a The [m^n ...] cage notation indicates n windows formed by m tetrahedral, T, atoms. ^b Silicon site atoms forming the cage. Si in bold indicates the minimum energy positions, and it can be seen that they correspond to what is experimentally found as shown in the right side figures. ^c The Si atoms that are pentacoordinated (to which the F⁻ is covalently bonded) are highlighted. ^d The fluoride location inside the D4R and [4¹5²6²] cages for the ITH structure, the [4³5⁴] cage for the STT structure, the [4³5²6¹] cage for the IFR structure, and the [4¹5²6²] cage for the STF structure are shown. The Si atoms experimentally reported to form the pentacoordinated unit have been highlighted. The cage notation appears below the figure. ^eExperimental fluoride locations are displayed.

units and two in the [4²6⁴] cages, called the IWR-D4R-[4²6⁴] distribution. A total number of 600 configurations were optimized (100 per each distribution set; see Table 2), and subsequently, the $E(\text{F,SDA})$ energy was calculated and represented in Table 3. It is interesting to note that the distributions containing D4R show lower energy than those not containing

D4R (IWR-[4²5⁴], IWR-[4¹5²6²], or IWR-[4²6⁴] distributions in Table 3). Thus, the lowest $E(\text{F,SDA})$ energies arise from the IWR-D4R-[4²5⁴], IWR-D4R-[4¹5²6²], and IWR-D4R-[4²6⁴] distribution sets. Although an important number of configurations belonging to the IWR-D4R-[4²6⁴] distribution present high energy values, this can be due to the fact that the D4R and

TABLE 5: Fluoride Incorporation Energy, E_{def} (eV), in the Pure Silica IWR Structure^e

structure	cage ^a	Si ^b	E_{def} (eV) ^c	F ⁻ location proposed ^d	
IWR	D4R	Si2	-3.3		
	[4 ² 5 ⁴]	Si3	-2.9		
		Si4	-3.2		
	[4 ¹ 5 ² 6 ²]	Si1	-3.3		
		Si3	-2.9		
		Si4	-3.2		

^a The [m^n ...] cage notation indicates n windows formed by m tetrahedral, T, atoms. ^b Silicon sites forming the cage. Si in bold indicates the minimum energy positions, and it can be seen that they correspond to what is experimentally found as shown in the right side figures. ^c A fluoride ion was placed in the close proximity of each Si atoms forming the cages in the pure silica structure. No organic SDA molecules were considered in the calculations. The energy was calculated using the Mott–Littleton methodology. ^d The Si atoms that are pentacoordinated (to which the F⁻ is covalently bonded) are highlighted. ^e The fluoride location in the [4²5⁴] (left) and [4¹5²6²] (right) cages is proposed.

[4²6⁴] are fused cages (see Figure 3), and it is possible that in some configurations the fluoride ions are located very closely, which could explain the higher energy values.

The lowest $E(\text{F}, \text{SDA})$ energies are displayed by IWR-D4R-distribution sets, so we think that two F⁻ ions will be located in the D4R units (two D4Rs per unit cell). The lowest $E(\text{F}, \text{SDA})$ energy values arise from the IWR-D4R-[4²5⁴] and ITH-D4R-[4¹5²6²] distribution sets (see Table 3), and therefore, the more intense ¹⁹F NMR peak (at -38 ppm) should correspond to D4R cages in agreement with NMR assignment.²⁸ As it is well established that D4R gives a signal at -38 ppm, then the signals at -59 and -81 ppm should correspond to the [4²5⁴] or [4¹5²6²] cages, according to our results (see Table 3) because the distribution IWR-D4R-[4²6⁴] is higher in energy than the IWR-D4R-[4²5⁴] and IWR-D4R-[4¹5²6²]. Discarding the higher energy configuration, F⁻ ions located in the [4²6⁴] cages can also be rationalized due to the electrostatic F⁻–F⁻ repulsion because D4R and [4²6⁴] are fused cages (see Table 3), and these repulsions may be making an important contribution and making the $E(\text{F}, \text{SDA})$ energy slightly larger (-2.2 eV) than in the other two distributions (-2.4 and -2.4 eV) corresponding to IWR-D4R-[4²5⁴] and IWR-D4R-[4¹5²6²]. Thus, the reported signal at -81 ppm assigned to F⁻ ions inside the [4²6⁴]²⁸ cannot be rationalized in view of our results, and we rather believe that the reported signals at -59 and -81 ppm should be assigned to F in the [4²5⁴] and [4¹5²6²] cages. This will be treated more in detail in the next section.

3.3. Short-Range F⁻–Framework Location. Once the F⁻ cage location has been established, we can study the fluoride bonding with the zeolite framework. For this purpose, one fluoride ion was introduced in pure silica IFR, ITH, IWR, STF, and STT structures as a defect using the Mott–Littleton methodology to study the Si–F bonding in each cage. The fluoride ion was introduced in close proximity to the different T sites present in the cages and the incorporation energies, E_{def} , obtained are shown in Table 4.

When the fluoride ions are introduced in the pure silica framework, a pentacoordinated silicon [SiO_{4/2}F]⁻ is formed except in the D4R cage where the fluoride is located in the cavity center.^{39,40} This corresponds to the experimental data where a pentacoordinated unit has been described for the pure silica ITH,²⁷ STT,^{16,22,52} IFR,^{16,32,34} and STF^{32,35} structures. The silicon site which has been described experimentally as forming

the pentacoordinated [SiO_{4/2}F]⁻ unit has been typed in bold in Table 4. A clear relationship can be found in Table 4 between Si atoms forming the pentacoordinated units and the lowest fluoride incorporation energies, E_{def} . For example, the [4¹5²6²] cage in the ITH structure is formed by three different Si atoms: Si6, Si7, and Si9 with energies -3.0, -3.1, and -3.0 eV, respectively (see Table 1). The lowest value, -3.1 eV, corresponds to the incorporation of the fluoride ion in the proximity of the Si7 position, which has been reported to form the pentacoordinated unit in the pure silica ITH structure.²⁷ In the STT structure, the [4³5⁴] cages are formed by 11 different Si atoms (Si4, Si5, Si6, Si7, Si9, Si11, Si12, Si13, Si14, Si15, and Si16). The fluoride atoms have been experimentally found bonded to three different atoms: Si7, Si12, and Si13. The calculated E_{def} range is between -2.6 and -3.2 eV, and the incorporation energies for Si7, Si12, and Si13 present the lowest values, -3.2, -3.1, and -3.2, respectively (see Table 4), which rationalizes the experimental findings in terms of energetic stability. A similar situation is observed in the case of the IFR structure whose [4³5²6¹] cages, where the fluoride ions have been located, are formed by four Si atoms: Si1, Si2, Si3, and Si4. The lowest calculated value, -3.2 eV, arises for Si3 and Si4 sites, and the experimental results show that the pentacoordinated silicon is at an Si4 site (see Table 4). The fluoride ion in the pure silica STF structure has been located linked to the Si3 atoms inside the [4¹5²6²] cage which shows, again, the lowest incorporation energy, E_{def} , -3.20 eV (see Table 4). We therefore, conclude that the F⁻ covalent bonding within the cage is dictated by an energetic criteria dominated by the short-range Si–F interactions. The minimum energy positions found by the defect calculations correspond to the experimentally found F⁻ location in the structures ITH, STT, IFR, and STF.

Finally, we simulated the fluoride incorporation energy in the pure silica IWR structure. The fluoride ions inside the D4R cage were located in the cavity center. If the fluoride ion is placed inside the [4²5⁴] cages, then the Si atoms with lowest incorporation energy, -3.2 eV, are the Si4 atoms (see Table 5). Conversely, when the fluoride atom is placed inside the [4¹5²6²] cage, then the pentacoordinated unit should be formed around the Si1 atoms, which present the lowest energy, -3.3 eV. This location of the fluoride ion in the IWR structure (Si1–F) is equivalent to that observed for the STF structure (Si3–F, see Table 4), where the ¹⁹F NMR signal has been reported at

−78 ppm³⁵ which is close to the reported signal at −81 ppm in the pure silica IWR structure.²⁸ The fluoride ions could therefore be distributed mainly in the D4R units and [4²5⁴] cages, and a small amount would be located in the [4¹5²6²] cages.

Coming back to our finding here, we stress the fact that the defect energetics of the F[−] location explains the Si–F bonding experimentally found. Previously, the cage in which the F[−] is located, when several possibilities are available, has to be calculated, and for that, we have seen that the *E*(F,SDA) terms were able to explain the F[−] cage occupation. It seems, therefore, as if the F[−] location is governed by a two step process. In a first stage, the electrostatic long-range forces, and especially the interactions between the F[−] and the SDA⁺ ions (including all the terms show in eq 13), decide which cages will be filled with F[−] ions and which cages will remain empty. From all the configurations possible, those giving the minimum *E*(F,SDA) energy (a term with a strong electrostatic contribution) have been found to reproduce the experimental F[−] cage occupation. In a second stage, once the F[−] ions are distributed in cages, the F[−] forms the covalent bonding with the Si site, within the corresponding cage, that gives the minimum defect energy, and this energy corresponds to the interaction between the F[−] ion and the zeolite framework, with no contribution of the interaction with the organic SDA.

4. Conclusions

A force field based methodology was used to study the fluoride distribution in the pure silica IFR, ITH, IWR, STF, and STT structures, which gives us greater knowledge about the role of fluoride ions in the synthesis of microporous materials. First, the fluoride distribution has been studied in the IFR, ITH, STF, and STT structures where the location has been reported using NMR and XRD techniques. The fluoride ions have been distributed inside the cages of the structures according to different distribution sets the SDAs being hosted in the main void volume of the zeolite framework, and full geometry optimization has been performed.

The cage in which the F[−] is reported experimentally, when several possibilities are available, has to be found, and for that, we have seen that the *E*(F,SDA) energy terms were able to explain the F[−] cage occupation due to the fact that the fluoride distributions observed experimentally show the lowest *E*(F,SDA) energies. Once the F[−] cage location was established, we then study the short-range fluoride–framework interactions, and for this purpose, one fluoride ion was introduced in the pure silica frameworks as a defect using Mott–Littleton methodology. A clear relationship was found between the Si atoms forming the pentacoordinated units and the lowest defect energies, *E*_{def}, which rationalizes the experimental findings in terms of energetic stability. It is suggested that, therefore, the F[−] location is governed by a two step process. First, the electrostatic interactions between the F[−] and the SDA⁺ ions (including all the terms show in eq 13) decide which cage will be filled with F[−] ions and which cages will remain empty. In a second stage, the F[−] bonds to the covalent bonding with the Si site to form the most stable pentacoordinated unit.

Moreover, this methodology was used to study the fluoride distribution in the pure silica structure IWR where the fluoride experimental location is not completely known. In view of our calculations, the fluoride could be distributed mainly in the D4R units and [4²5⁴] cages and a small amount will be located in the [4¹5²6²] cages, making it possible to rationalize the ¹⁹F NMR chemical shifts observed experimentally in the pure silica structure.

Acknowledgment. Financial support from the Ministerio de Educación y Ciencia through project MAT2003-07769-C02-01 is acknowledged. A.P. thanks BANCAJA-CSIC for a PhD grant. CPD-UPV (Centro de Proceso de Datos—Universidad Politécnica de Valencia) is acknowledged for the use of their computational facilities.

References and Notes

- (1) Corma, A. *J. Catal.* **2003**, *216*, 406–416.
- (2) Barrer, R. M. *Hydrothermal Chemistry of Zeolites*; Academic Press, London, 1982.
- (3) Flanigen, E. M.; Patton, R. L. U.S. Patent 4,073,865, 1978.
- (4) Blasco, T.; Cambor, M. A.; Corma, A.; Esteve, P.; Guil, J. M.; Martínez, A.; Perdigon-Melon, J. A.; Valencia, S. *J. Phys. Chem. B* **1998**, *102*, 75–88.
- (5) Guth, J. L.; Kessler, H.; Caullet, P.; Hazm, J.; Merrouche, A.; Patarin, J. A multifunctional tool for microporous solids-mineralizing, structure directing and templating effects in the synthesis, *Proceedings of the 9th International Zeolite Conference*; Montreal, 1992; von Ballmoos, R., Higgins, J. B., Treacy, M. M. J., Eds.; Butterworth-Heinemann: Boston, MA; pp 215–222.
- (6) Delmotte, L.; Soudard, M.; Guth, F.; Seive, A.; López, A.; Guth, J. L. *Zeolites* **1990**, *10*, 778–783.
- (7) Estermann, M.; McCusker, L. B.; Baerlocher, Ch.; Merrouche, A.; Kessler, H. *Nature* **1991**, *352*, 320–323.
- (8) Kuperman, A.; Nadimi, S.; Oliver, S.; Ozin, G. A.; Garces, J. M.; Olken, M. M. *Nature* **1993**, *365*, 239–242.
- (9) Axon, S. A.; Klinowski, J. *Appl. Catal. A* **1992**, *81*, 27–34.
- (10) Cambor, M. A.; Villaescusa, L. A.; Díaz-Cabañas, M. J. *Top. Catal.* **1999**, *9*, 59–76.
- (11) Guth, J. L.; Kessler, H.; Wey, R. New route to pentasil-type zeolites using a nonalkaline medium in the presence of fluoride ions, In *New Developments in Zeolite Science and Technology, Proceedings of the 7th International Zeolite Conference*; Tokyo, 1986; Murakami, Y., Iijima, A., Ward, J. W., Eds.; Kodansha Ltd.: Tokyo and Elsevier: Amsterdam; pp 121–128.
- (12) George, A. R.; Catlow, C. R. A. *Zeolites* **1997**, *18*, 67–70.
- (13) Sastre, G.; Gale, J. D. *Chem. Mater.* **2005**, *17*, 730–740.
- (14) Attfield, M. P.; Catlow, C. R. A.; Sokol, A. A. *Chem. Mater.* **2001**, *13*, 4708–4713.
- (15) Koller, H.; Wolker, A.; Valencia, S.; Villaescusa, L. A.; Díaz-Cabañas, M. J.; Cambor, M. A. ¹⁹F and ²⁹Si solid-state NMR spectroscopy on five-coordinate silicon sites, (SiO)₄SiF[−], in zeolites, *Proceedings of the 12th International Zeolite Conference*; Baltimore, 1998; Treacy, M. M. J., Marcus, B. K., Bisher, M. E., Higgins, J. B., Eds.; Materials Research Society: Warrendale, PA; pp 2951–2954.
- (16) Koller, H.; Wolker, A.; Villaescusa, L. A.; Díaz-Cabañas, M. J.; Valencia, S.; Cambor, M. A. *J. Am. Chem. Soc.* **1999**, *121*, 3368–3376.
- (17) Koller, H.; Wolker, A.; Eckert, H.; Panz, C.; Behrens, P. *Angew. Chem., Int. Ed.* **1997**, *36*, 2823–2825.
- (18) Fyfe, C. A.; Lewis, A. R.; Chezeau, J. M.; Grondey, H. *J. Am. Chem. Soc.* **1997**, *119*, 12210–12222.
- (19) Fyfe, C. A.; Brouwer, D. H.; Lewis, A. R.; Chezeau, J. M. *J. Am. Chem. Soc.* **2001**, *123*, 6882–3891.
- (20) Barrett, P. A.; Díaz-Cabañas, M. J.; Cambor, M. A.; Jones, R. H. *J. Chem. Soc., Faraday Trans.* **1998**, *94*, 2475–2481.
- (21) van der Goor, G.; Freyhardt, C.; Behrens, P. *Z. Anorg. Allg. Chem.* **1995**, *621*, 311–322.
- (22) Cambor, M. A.; Díaz-Cabañas, M. J.; Pérez-Pariente, J.; Teat, S. J.; Clegg, W.; Shannon, I. J.; Lightfoot, P.; Wright, P. A.; Morris, R. E. *Angew. Chem., Int. Ed.* **1998**, *37*, 2122–2126.
- (23) Price, G. D.; Pluth, J. J.; Smith, J. V.; Bennett, J. M.; Patton, R. L. *J. Am. Chem. Soc.* **1982**, *104*, 5971–5977.
- (24) Mentzen, B. F.; Sacerdote-Peronet, M.; Guth, J. L.; Kessler, H. C. *R. Acad. Paris Ser. II* **1991**, *131*, 177.
- (25) Caullet, P.; Guth, J. L.; Hazm, J.; Lamblin, J. M.; Gies, H. *Eur. J. Solid State Inorg. Chem.* **1991**, *28*, 345–361.
- (26) Villaescusa, L. A.; Barret, P. A.; Cambor, M. A. *Angew. Chem., Int. Ed.* **1999**, *38*, 1997–2000.
- (27) Corma, A.; Puche, M.; Rey, F.; Sankar, G.; Teat, S. J. *Angew. Chem., Int. Ed.* **2003**, *42*, 1156–1159.
- (28) Cantín, A.; Corma, A.; Díaz-Cabañas, M. J.; Jordá, J. L.; Moliner, M. J. *J. Am. Chem. Soc.* **2006**, *128*, 4216–4217.
- (29) Baerlocher, Ch.; Meier, W. M.; Olson, D. H. *Atlas of Zeolite Framework Types*, 5th ed.; Elsevier: Amsterdam, 2001; <http://www.iza-online.org>.
- (30) Bull, I.; Villaescusa, L. A.; Teat, S. J.; Cambor, M. A.; Wright, P. A.; Lightfoot, P.; Morris, R. E. *J. Am. Chem. Soc.* **2000**, *122*, 7128–7129.
- (31) Attfield, M. P.; Weigel, S. J.; Taulelle, F.; Cheetham, A. K. *J. Mater. Chem.* **2000**, *10*, 2109–2113.

- (32) Villaescusa, L. A.; Wheatley, P. S.; Bull, I.; Lighfoot, P.; Morris, R. E. *J. Am. Chem. Soc.* **2001**, *123*, 8797–8805.
- (33) Darton, R. J.; Brouwer, D. H.; Fyfe, C. A.; Villaescusa, L. A.; Morris, R. E. *Chem. Mater.* **2004**, *16*, 600–603.
- (34) Barrett, P. A.; Cambor, M. A.; Corma, A.; Jones, R. H.; Villaescusa, L. A. *J. Phys. Chem. B* **1998**, *102*, 4147–4155.
- (35) Fyfe, C. A.; Brouwer, D. H.; Lewis, A. R.; Villaescusa, L. A.; Morris, R. E. *J. Am. Chem. Soc.* **2002**, *124*, 7770–7778.
- (36) Arranz, M.; Pérez-Pariente, J.; Wright, P. A.; Slawin, A. M. Z.; Blasco, T.; Gómez-Hortigüela, L.; Corà, F. *Chem. Mater.* **2005**, *17*, 4374–4385.
- (37) (a) Gale, J. D. *J. Chem. Soc., Faraday Trans.* **1997**, *93*, 629–637. (b) Gale, J. D.; Rohl, A. L. *Mol. Simul.* **2003**, *29*, 291–341.
- (38) Wagner, P.; Zones, S. I.; Davis, M. E.; Medrud, R. C. *Angew. Chem., Int. Ed.* **1999**, *38*, 1269–1272.
- (39) Sastre, G.; Pulido, A.; Corma, A. *Chem. Commun.* **2005**, 2357–2359.
- (40) Pulido, A.; Sastre, G.; Corma, A. *Chem. Phys. Chem.* **2006**, *7*, 1092–1099.
- (41) Kiselev, A. V.; Lopatkin, A. A.; Shulga, A. A. *Zeolites* **1985**, *5*, 261–267.
- (42) Oie, T.; Maggiora, T. M.; Christoffersen, R. E.; Duchamp, D. J. *Int. J. Quantum Chem., Quantum Biol. Symp.* **1981**, *8*, 1–47.
- (43) Lewis, D. W.; Freeman, C. F.; Catlow, C. R. A. *J. Phys. Chem.* **1995**, *99*, 11194–11202.
- (44) Lewis, D. W.; Catlow, C. R. A.; Thomas, J. M. *Chem. Mater.* **1996**, *8*, 1112–1118.
- (45) Catlow, C. R. A.; Bell, R. G.; Gale, J. D. *J. Mater. Chem.* **1994**, *4*, 781–792.
- (46) Sastre, G.; Lewis, D. W.; Catlow, C. R. A. *J. Phys. Chem.* **1996**, *100*, 6722–6730.
- (47) Sastre, G.; Lewis, D. W.; Catlow, C. R. A. *J. Phys. Chem. B* **1997**, *101*, 5249–5262.
- (48) Sastre, G.; Pulido, A.; Castañeda, R.; Corma, A. *J. Phys. Chem. B* **2004**, *108*, 8830–8835.
- (49) Barrett, P. A.; Cambor, M. A.; Corma, A.; Jones, R. H.; Villaescusa, L. A. *Chem. Mater.* **1997**, *9*, 1713–1715.
- (50) Castañeda, R.; Corma, A.; Fornés, V.; Rey, F.; Rius, J. *J. Am. Chem. Soc.* **2003**, *125*, 7820–7821.
- (51) (a) Wagner, P.; Zones, S. I.; Medrud, R. C.; Davis, M. E. *Abstr. Pap.—12th Int. Zeolite Conf.* (Baltimore, MD) **1998**. (b) Nakagawa, Y. (Chevron Research and Technology Company), US-A 5316753. *Chem. Abstr.* **1994**, *121*, 112714j.
- (52) Cambor, M. A.; Díaz-Cabañas, M. J.; Cox, P. A.; Shannon, I. J.; Wright, P. A.; Morris, R. E. *Chem. Mater.* **1999**, *11*, 2878–2885.